

Melt Pool Evolution Study in Selective Laser Melting

Bo Cheng and Kevin Chou

Mechanical Engineering Department
The University of Alabama
Tuscaloosa, AL 35487

REVIEWED

Abstract

In selective laser melting (SLM) additive manufacturing, the completion of the entire scanning cross-sectional area of each layer build is consisted of many smaller scanning patches. Hence, the scanning length in each path may be too short to reach the melt pool quasi-steady state, thus, affecting the melt pool geometry, which is also effected by the process parameters. It is also known that the melt pool size correlates with the build part microstructures and properties. In this study, temperature simulations, finite-element based, of SLM for In718 is applied to track the thermal response during scanning of an individual patch. The results show that the process parameters determine the melt pool evolution, which affects the actual molten pool size in the regions defined by the raster scanning length. Manipulating the scanning path length and process parameters, based on the melt pool evolution information, may help to achieve a desired melt pool size for part quality controls.

Keywords: Selective laser melting, raster scan, finite element method, remelting.

1. Introduction

Powder-bed selective laser melting (SLM) is one of the additive manufacturing processes where metal parts are made directly from 3D CAD data without any special tooling in a layer by layer fashion. During the SLM process, a desired part is fabricated by selectively melting successive layers of powder materials using a high energy laser beam on a support platform. The top powder layer is melted and forms moving liquid pool. Then, the melted material solidifies quickly and starts to form the desired shape. After the completion of the designed cross-section scan of a layer, the platform is lowered down by one layer thickness for new powder layer deposition. This deposition-scanning process is repeated until the whole part is finished building. The unused powder can be retrieved and reused in next build after the fabricating process. The whole building process is usually conducted in a chamber filled with inert gas [1]. SLM technology has many advantages in comparison with other methods for manufacturing parts with complex geometry and inner structure. SLM is also capable of producing objects with mechanical properties comparable to those of bulk materials and to offer significant time savings by considerably reducing post-processing steps [2-4].

SLM has been widely applied with commercial materials such as stainless steel [5] and iron [6]. Among all the materials, Inconel718 is a niobium-modified nickel-base super-alloy which has been widely used in aeronautic, astronautic and nuclear industries for its good strength, excellent resistance to oxidation at high temperatures, and favorable weldability [7]. It is widely

used to fabricate parts used in critical environments because it has high strength up to 923 K, as well as good corrosion resistance and creep resistance [8]. While complex structures, such as internal channel, are difficult to make by traditional methods such as casting and machining, SLM is a promising alternative method.

Despite many potential advantages over conventional manufacturing technologies, SLM still encounters several part and process defects due to high energy input such as rough surface finish and severe deformation. In the building process, some of the SLM systems utilize a patch scanning strategy in which the completion of the entire scanning cross-sectional area of each layer is consists of many smaller scanning patches, as shown in Figure 1. The system randomly picked the patches to do hatch scanning and the scanning direction is different for adjacent patches, e.g., rotated by 90 degree between neighboring patches. The melt pool will reach quasi-steady state after beam travels certain distance that its geometry will keep unchanged in the following scanning. Hence, the scanning length in each path may be too short to reach the quasi-steady state, thus, affecting the melt pool geometry, which is also effected by the process parameters. It is also known that the melt pool size correlates with the build part microstructures and properties. In addition, the solidified material remelting phenomenon caused by melt pool geometry may also be quite influential to part quality such as porosity reduction [9] and minimization of macro-segregation defect [10]. However, excessive remelting may deteriorate part surface quality [11].

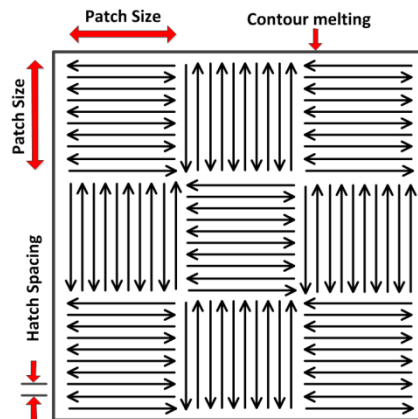


Figure 1. Patch scanning strategy.

Therefore, physics-based modeling of SLM process phenomena is required to investigate process characteristics such as melt pool sizes and temperature fields. Thermal models have been widely investigated in powder bed metal additive manufacturing studies. Song et al [12] has reported a 3D SLM model to simulate the temperature distribution with a surface Gaussian heat source. Dong et al [13] developed a finite element model of polycarbonate material to study the phase transformation during the selective laser sintering (SLS) process. The process parameters effects on temperature have been investigated. Xing et al [14] developed a SLS 3D model for Al_2O_3 coated ceramic powder to simulate the transient temperature. Experiment with high-speed CCD temperature collection was used for model validation. Yuan and Gu [15] established a 3D finite volume method (FVM) model to investigate the temperature evolution behaviour and fluid flow effect in melt pool during SLM process of TiC/AlSi10Mg material. Zeng et al [16] have presented a comprehensive literature review of SLM/SLS thermal analysis. Information about

SLM analytical solution, numerical modeling works, temperature measurements and examples of simulation results has been detailed. However, the modeling studies of the SLM process for In718 material have been relatively rare. Schilp et al [17] presented both microscale and macroscale models to study the temperature distribution in a laser beam melting of In718. The temperature distribution and its temporal evolution can be investigated by the developed model.

In this study, a finite element model incorporating Gaussian heat flux distribution and raster scan strategy was developed to study the melt pool evolution phenomenon in one scanning patch. The model can be utilized to track the thermal characteristics under given process parameters and raster length. The objective of this task is to have fundamental understanding of the In718 SLM thermal characteristics such as temperature distributions and melt pool sizes for its widespread applications.

2. Selective laser melting model construction

2.1 Governing equation

In the SLM process, a laser beam travels along raster pattern on the surface of the powder layer at a constant speed. The instantaneous temperature distribution satisfies the following 3D heat transport conduction equation:

$$\nabla \left(\frac{k}{\rho c} \nabla T \right) + \frac{\dot{Q}}{\rho c} = \frac{\partial T}{\partial t} + v \frac{\partial T}{\partial x} \quad (1)$$

where T is temperature, \dot{Q} is the absorbed heat flux, c is specific heat capacity, ρ is density, k is thermal conductivity, v is the constant scanning speed.

In order to improve the numerical modeling accuracy, the latent heat of fusion, L_f , was also considered in this study. It was implemented as an additional term of the internal thermal energy per unit mass, when the temperature is between the solidus and liquidus temperature. The enthalpy, $H(T)$, can be defined as follows:

$$H(T) = \int c dT + L_f f \quad (2)$$

where f is the volumetric fraction of the liquid:

$$f = \begin{cases} 0 & T < T_s, \\ \frac{T - T_s}{T_L - T_s} & T_s \leq T \leq T_L, \\ 1 & T > T_L \end{cases} \quad (3)$$

2.2 Heat input equation

A thermal mathematical model with high accuracy is critical to simulate the input laser heat source in SLM scanning process. In this study, the laser beam heat input distribution is modeled as a conical moving heat source with a Gaussian distribution and linearly decaying along the beam penetrating direction [18]:

$$\dot{Q}_{(x,y,z)} = \eta \times \frac{H_s \times I_z}{s} \quad (4)$$

with

$$I_z = \frac{1}{0.75} \left(-2.25 \left(\frac{z}{S} \right)^2 + 1.5 \left(\frac{z}{S} \right) + 0.75 \right),$$

$$H_s = \frac{2UI_b}{\pi \Phi_E^2} \exp \left\{ -\frac{2[(x-x_s)^2 + (y-y_s)^2]}{\Phi_E^2} \right\}.$$

Where the parameters include Gaussian heat source: H_s , the linearly decaying function: I_z , laser beam efficiency coefficient: η , voltage: U , current: I_b , penetration depth: S , beam diameter: Φ_E , and the instantaneous horizontal position of the heat source center: x_s and y_s . User subroutine, DFLUX, is programmed to incorporate incident heat flux in the simulation process.

2.3 Material properties

Temperature dependent material properties were incorporated in the numerical study since a wide range of temperature should be expected during high energy laser melting process. Temperature dependent properties such as density, specific heat and conductivity of solid In718 alloy have been reported in literature [19], and summarized in Figure 2. The increase of thermal conductivity after melting point is used to simulate the heat convection of melt pool [20].

Since the incident laser beam heat source is directly applied in the top powder layer of scanned region, it is critical to take into account of the powder property in the calculation process due to significant difference of thermal properties between powder and solid bulk material [18]. The latent heat of fusion and specific heat of powder may be considered the same as those of the solid material [21-27]. Moreover, the powder material may have the same properties of solid bulk material after being melted. The density of the powder material can be calculated through a function of the local powder density and the solid material density [28]:

$$\Phi = \frac{\rho_{bulk} - \rho_{powder}}{\rho_{bulk}} \quad (5)$$

where Φ is the powder porosity; ρ_{bulk} and ρ_{powder} are the solid and powder densities, respectively.

There are studies of the thermal conductivity of powder in recent years, including both theoretical and experimental methods. Tolochko et al. [27] developed a thermal conductivity model for Ti powder in a study of SLS process. The effective powder thermal conductivities due to radiation and powder particle necks have been considered in the model. Cheng et al [18] utilized a TPS2500S thermal analyzer to experimentally calibrate the conductivity of Ti-6Al-4V at different temperatures. In this study, the powder thermal conductivity is considered according to the ratio of Ti-6Al-4V solid and powder conductivity value [18], as shown in Figure 2. Material state change, e.g., powder to solid, is also considered and programmed in user subroutine UMATHT. The state change criterion is that powder material is melted and under cooling.

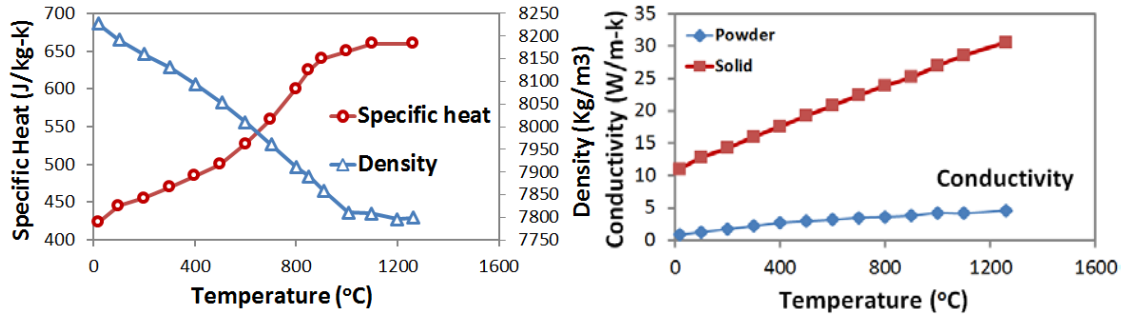


Figure 2. In718 thermal properties [19].

2.4 Model configuration

A 3D finite element method (FEM) thermal model was developed to investigate the thermal process of SLM by commercial software ABAQUS. Raster scan path was simulated in this model, thus the previous deposited material was modeled as solid. The newly deposited powder layer on the top surface of deposited material was considered and has the powder thermal properties. The beam heating starts at the top powder surface and travels along the designed raster path with a constant speed. The initial condition for the whole computational domain has been set to be a uniform temperature of $T_{initial}$. The thermal boundary conditions for heat losses due to surface convection and radiation on the top surface have also been considered in the model. The 3D simulation model is presented in Figure 3. The solid substrate for the model was a block of In718 bulk material with dimensions of 8 mm × 8 mm × 10.7 mm in (x, y, z) direction. Considering the calculation efficiency and computational precision, heat transfer elements (DC3D8) elements with a fine mesh of 0.035 mm × 0.035 mm × 0.015 mm ($x \times y \times z$), were used to represent the raster scanning region, while a relatively coarse mesh was adopted for the substrate. The laser beam moved in a raster pattern, the highlighted region in Figure 3 is the designed scanning region. The specific raster scan type is programmed in user subroutine “DFLUX” by defining the heat source center location moving along the raster path as a function of time. Detailed process modeling and simulation parameters are listed in Table 1.

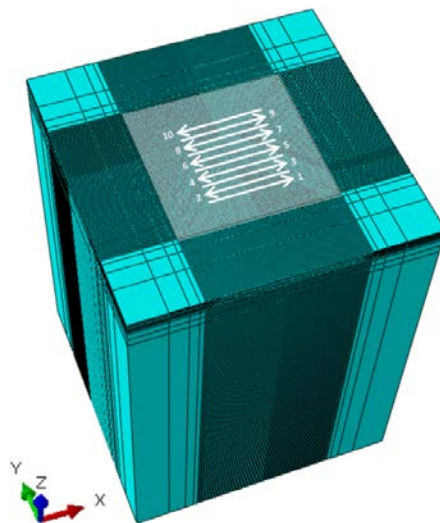


Figure 3. An example of 3D FEM model for multi-path scanning with fine mesh.

Table 1. Parameter List Used in Simulations For In718.

Parameters	Values
Solidus temperature, T_S (°C)	1260 [29]
Liquidus temperature, T_L (°C)	1336 [29]
Latent heat of fusion, L_f (kJ/Kg)	227 [30]
Beam diameter, Φ (mm)	0.15
Absorption efficiency, η	0.364 [31]
Scan speed, v (mm/sec)	1000
Beam power, P (W)	450
Powder layer thickness, t_{layer} (mm)	0.03
Porosity, ϕ	0.5
Beam penetration depth, d_P (mm)	0.062 [21]
Thermal initial condition, $T_{initial}$ (°C)	100 [12]
Emissivity, ε	0.3 [32]
Convection coefficient, h (W/m ² -k)	10 [33]

3. Results and Discussion

3.1 Model Validation

Due to lack of available experimental data for In718 in SLM process, a thermal process research study by Cheng et al [18] in the field of the Electron Beam Additive Manufacturing (EBAM) process of Ti-6Al-4V was used for model validation and correction purposes. The two additive manufacturing processes are similar; the major differences between EBAM process and SLM process are the thermal boundary conditions, e.g., much higher preheating temperature and no convection in EBAM. The simulation results of the model, including temperature contours, temperature profile along scanning path and melt pool sizes were compared with experimentally obtained data. The simulated results agree well with experiments, thus it is reasonable to utilize the model to do thermal analysis of laser scanning process based on thermal boundary condition adjustments. The detailed validation process can be found in literature [18].

3.2 Typical example of simulated results

Simulations have been conducted by moving the laser beam along raster pattern, as shown in Figure 3. This raster pattern in a single patch may contribute to understand temperature distribution of a single layer. The raster patch consisted of 10 straight paths with length=1 mm, they have been connected by raster turning arms with length=105 μ m (hatch spacing). An initial calculation was run with 0.15 mm beam diameter, 1000 mm/s scanning speed and 450 W laser power. The temperature distribution, at different scanning time, on the top powder layer is shown in Figure 4, where the geometry of the melt pool is plotted with the threshold value of the liquidus point of In718 with blank color. The temperature evolution clearly shows the moving melt pool is followed by the just solidified material with decreasing temperature, as shown in Figure 4-a. Melt pool temperature starts to increase again when the laser beam reaches the turning point of the raster path and travels along the short raster connection arm. It is noted the melt pool max temperature has increased from 1968 to 2086 °C in Figure 4-b. Then, the laser beam travels along the second straight raster path. At this point, partial solidified material in the

first scanning path may start to be remelted because the input laser power is affected by previous residual heat that has not fully dissipated to substrate solid material. The melt pool max temperature is still higher than that of the first scanning path. In addition, the melt pool size is increased by residual heat effect, as shown in Figure 4-c. Moreover, Figure 4-d indicates that when the laser beam continues to travel, the melt pool size and max temperature may decrease due to the residual heat effect of first scanning path reduces with time increases.

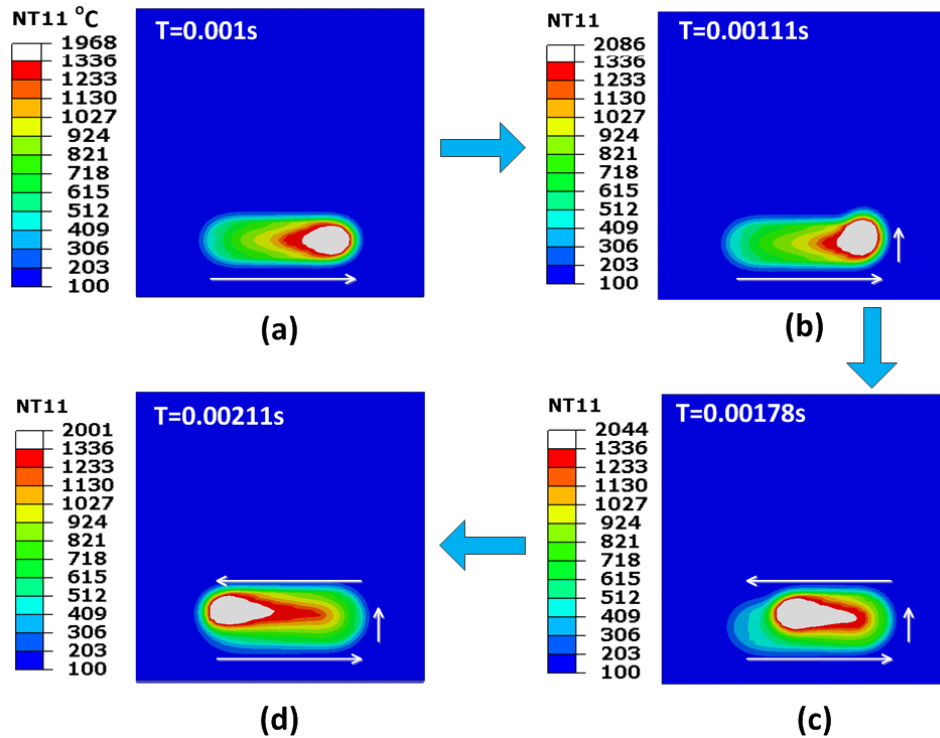


Figure 4. Example of temperature and melt pool evolution in raster scan.

Further observations have indicated that the residual heat would further increase the melt pool size when laser beam travels on the subsequent scanning paths. When the laser beam passes certain raster path, the residual heat effect may come to a balance and the max melt pool size will not further increase, as shown in Figure 5-a. Figure 5-b illustrates the melt pool shape when the laser beam travels along different raster paths. It can be noted when the beam is travelling along path 1 the melt pool is symmetric to the path centerline. However, when the laser beam travels along path 5, the melt pool is not symmetric, a larger half of melt pool area is shown on the residual heat effect region.

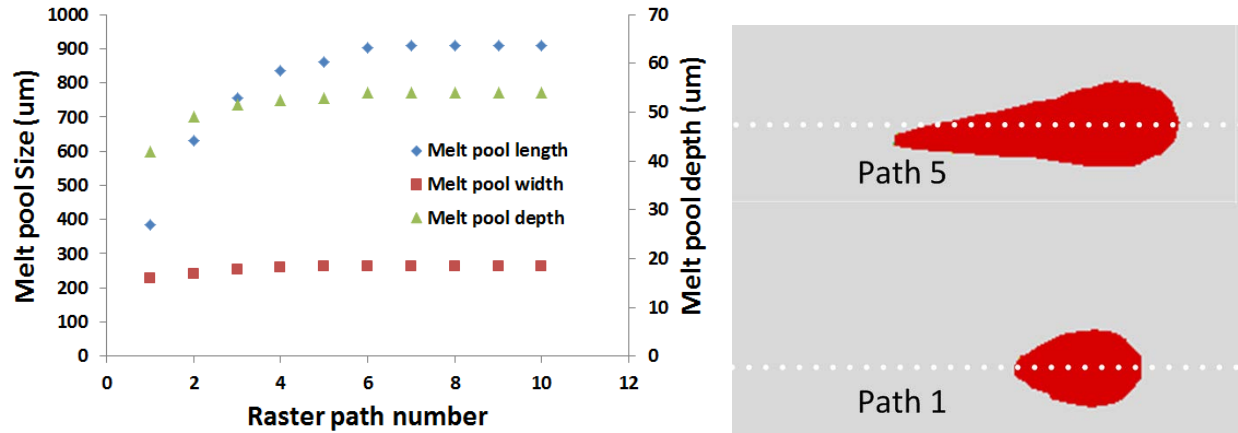


Figure 5. (a) Max melt pool size in different raster path, (b) melt pool shape.

3.3 Raster length effect on melt pool evolution

The melt pool evolution process information in single track scanning has been collected and summarized in Figure 6. It is observed that melt pool will start to form after laser beam moves a very short distance. Melt pool sizes will continue to increase until reach steady state. It is also noted that the melt pool depth and width will reach steady state ahead of length. The melt pool length will get fully developed at around 0.55 mm under current given process parameters. If laser beam travels in a smaller path region, the scanning length in each path may be too short to reach the quasi-steady state, thus, affecting the melt pool geometry. Therefore, A smaller raster length case, length=0.5 mm has been conducted to evaluate the raster length effect on melt pool geometry. The raster region consisted of 5 straight paths due to the reduction of scanning length. The residual heat effect is expected to be more serious since a smaller region reduces the heat dissipating time. The incident heat input region will overlap with the residual heat region thus increase the possibility of forming larger remelting zone. Figure 7 shows the melt pool shapes at raster path 1, 3, 5 for different raster length cases. The melt pool length of the L=0.5 mm case is smaller than that of L=1 mm due to the restriction of shorter scanning track. However, the width of lower half of the melt pool increases significant due to residual heat effect after laser beam scanned several paths, e.g., melt pool in path 5, as shown in Figure 7 for L=0.5 mm case.

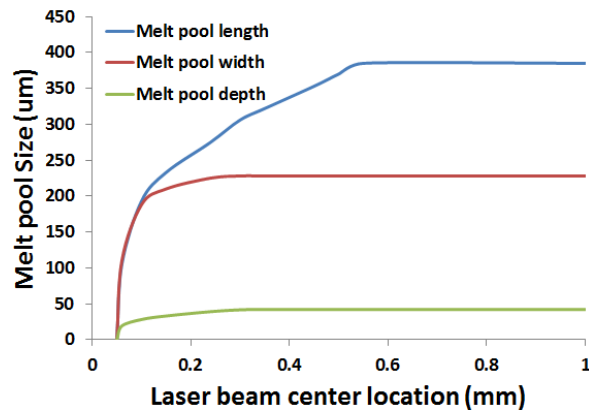


Figure 6. Melt zone maps for the first five paths

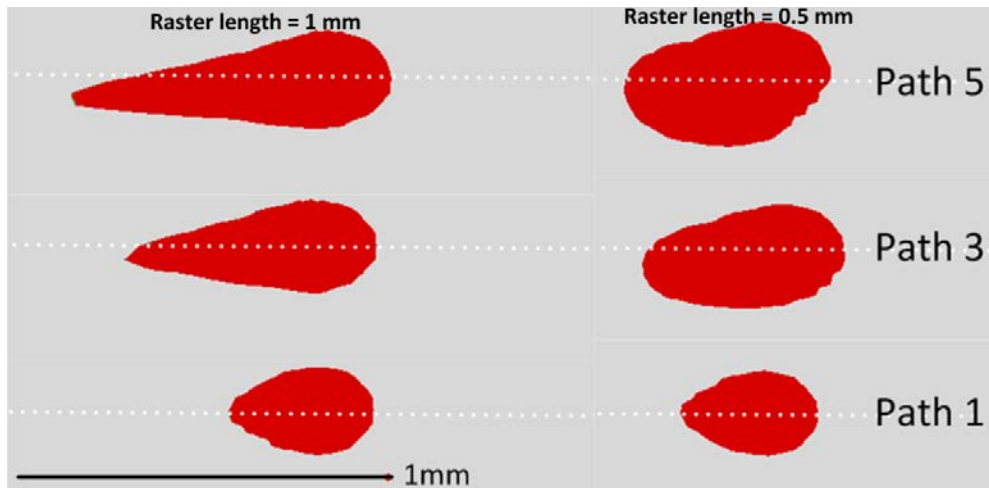


Figure 7. Melt pool size in different scanning path

3.4 Process parameters effect

It is well known that different parameters may affect melt pool geometry, cooling rate, grain growths, residual stresses and deformation, and may also play a critical role in part microstructure as well as hardness and elastic properties [34-37]. Therefore, it is necessary to investigate their effects on raster scan. Figure 8 shows the melt pool length evolution process for different process parameters simulation results. The results have displayed interesting characteristics: (1) higher beam power as well as slower beam speed cases may need longer scanning length to reach melt pool steady state, e.g., case (3), (4) vs. case (1); (2) a smaller beam diameter may reduce the scanning length needed for melt pool fully development, e.g., case (2) vs. case (1). Thus, the interesting phenomenon may also greatly affect the melt pool evolution in raster scanning. It is observed that, for case (1) and (2) in Figure 9-a and b, the raster length may have minor effect on melt pool geometry since the melt pool needs a distance shorter than 0.5 mm to get steady state. Thus the residual heat may have minor effect on succeeding melt pool evolution. For case (3) in Figure 9-c, the necessary length for melt pool fully development is around 0.5 mm. Therefore the residual heat effect on melt pool geometry can not be ignored, it is noted that the accumulated residual heat has noticeably expanded the melt pool width. The observed melt pool shape changes from comet-like to more ellipse-like, especially for the lower half of the melt pool.

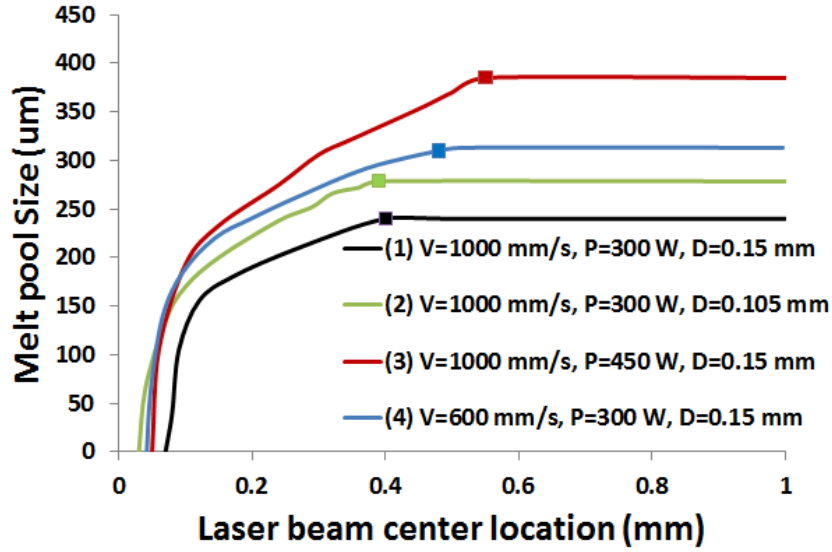


Figure 8. Melt pool length evolution for different process parameters.

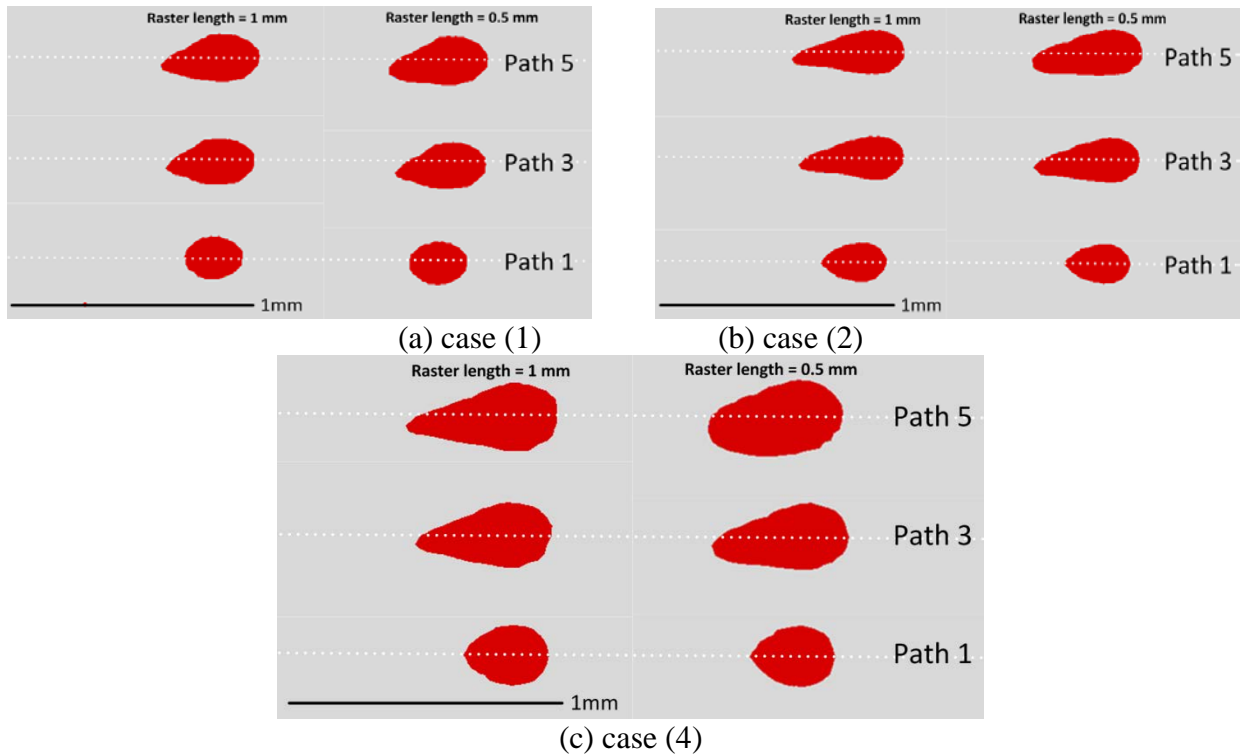


Figure 9. Raster length effect on different process parameters cases.

4. Conclusion

This study focuses on the development of a numerical thermal model for In718 SLM process. A 3D thermal model, using finite element method, was developed for SLM process thermal behavior simulations under different patch scanning conditions. The model incorporated a moving heat source with a Gaussian volumetric intensity, In718 powder as well as solid

material temperature-dependent properties and raster scan strategy, etc. The major findings can be summarized as follows.

(1) The residual heat will significantly affect the melt pool size during raster scan, the melt pool will increase during the raster scanning process. However, the residual heat effect may reach a steady state and the max melt pool size keeps the same after the laser beam passes certain raster path, e.g., path 6 in this study for $V=1000$ mm/s, $P=450$ W, $D=0.15$ mm case.

(2) Process parameters will significantly affect melt pool development, a larger beam power and slower beam speed can increase the traveling distance for a full evolution while a smaller beam diameter may reduce this distance.

(3) In the regions defined by the raster scanning length, a longer melt pool evolution distance may have a more significant effect on the melt pool geometry on the subsequent raster scanning path.

Future work of this research will require temperature and melt pool measurements for comprehensive model validations. The current initial and boundary conditions need to be better defined by actual experiment results. In the current study, the SLM model was validated by EBAM process, and further validation from SLM machine experiment is needed to improve model prediction accuracy.

Acknowledgment

This research is supported by NASA, No. NNX11AM11A. The first author acknowledges the scholarship support from the Alabama EPSCoR Graduate Research Scholars Program.

References

- [1] Thijs, L., Verhaeghe, F., Craeghs, T., Van Humbeeck, J., and Kruth, J.-P., 2010, "A study of the microstructural evolution during selective laser melting of Ti-6Al-4V," *Acta Materialia*, 58(9), pp. 3303-3312.
- [2] Yadroitsev, I., Shishkovsky, I., Bertrand, P., and Smurov, I., 2009, "Manufacturing of fine-structured 3D porous filter elements by selective laser melting," *Applied Surface Science*, 255(10), pp. 5523-5527.
- [3] Bourell, D., Wohler, M., Harlan, N., Das, S., and Beaman, J., 2002, "Powder densification maps in selective laser sintering," *Advanced Engineering Materials*, 4(9), pp. 663-669.
- [4] Kruth, J.-P., Levy, G., Klocke, F., and Childs, T., 2007, "Consolidation phenomena in laser and powder-bed based layered manufacturing," *CIRP Annals-Manufacturing Technology*, 56(2), pp. 730-759.
- [5] Wang, L., and Felicelli, S., 2007, "Process modeling in laser deposition of multilayer SS410 steel," *Journal of Manufacturing Science and Engineering*, 129(6), pp. 1028-1034.
- [6] Kruth, J.-P., Froyen, L., Van Vaerenbergh, J., Mercelis, P., Rombouts, M., and Lauwers, B., 2004, "Selective laser melting of iron-based powder," *Journal of Materials Processing Technology*, 149(1), pp. 616-622.
- [7] Zhao, X., Chen, J., Lin, X., and Huang, W., 2008, "Study on microstructure and mechanical properties of laser rapid forming Inconel 718," *Materials Science and Engineering: A*, 478(1), pp. 119-124.

- [8] Liu, L., Hirose, A., and Kobayashi, K. F., 2002, "A numerical approach for predicting laser surface annealing process of Inconel 718," *Acta materialia*, 50(6), pp. 1331-1347.
- [9] Gong, H., Rafi, K., Gu, H., Starr, T., and Stucker, B., 2014, "Analysis of defect generation in Ti-6Al-4V parts made using powder bed fusion additive manufacturing processes," *Additive Manufacturing*, 1, pp. 87-98.
- [10] Van Den Avyle, J. A., Brooks, J. A., and Powell, A. C., 1998, "Reducing defects in remelting processes for high-performance alloys," *JOM*, 50(3), pp. 22-25.
- [11] Guo, C., Ge, W., and Lin, F., 2014, "Material Molten Time and its Effect on Material Deposition during Electron Beam Selective Melting," 25th Annual International Solid Freeform Fabrication Symposium - An Additive Manufacturing Conference, Austin, TX, USA, August 4-6, 2014.
- [12] Song, B., Dong, S., Liao, H., and Coddet, C., 2012, "Process parameter selection for selective laser melting of Ti6Al4V based on temperature distribution simulation and experimental sintering," *The International Journal of Advanced Manufacturing Technology*, 61(9-12), pp. 967-974.
- [13] Dong, L., Makradi, A., Ahzi, S., and Remond, Y., 2009, "Three-dimensional transient finite element analysis of the selective laser sintering process," *Journal of materials processing technology*, 209(2), pp. 700-706.
- [14] Xing, J., Sun, W., Rana, R., and IEEE, S. M., 2013, "3D modeling and testing of transient temperature in selective laser sintering (SLS) process," *Optik-International Journal for Light and Electron Optics*, 124(4), pp. 301-304.
- [15] Yuan, P., and Gu, D., 2015, "Molten pool behaviour and its physical mechanism during selective laser melting of TiC/AlSi10Mg nanocomposites: simulation and experiments," *Journal of Physics D: Applied Physics*, 48(3), p. 035303.
- [16] Zeng, K., Pal, D., and Stucker, B., 2012, "A review of thermal analysis methods in Laser Sintering and Selective Laser Melting," 23rd Annual International Solid Freeform Fabrication Symposium - An Additive Manufacturing Conference, Austin, TX, USA, August 6-8, 2012.
- [17] Schilp, J., Seidel, C., Krauss, H., and Weirather, J., 2014, "Investigations on Temperature Fields during Laser Beam Melting by Means of Process Monitoring and Multiscale Process Modelling," *Advances in Mechanical Engineering*, 2014, p. 7.
- [18] Cheng, B., Price, S., Lydon, J., Cooper, K., and Chou, K., 2014, "On Process Temperature in Powder-Bed Electron Beam Additive Manufacturing: Model Development and Validation," *Journal of Manufacturing Science and Engineering*, 136(6), pp. 061018-061018.
- [19] Dye, D., Hunziker, O., Roberts, S., and Reed, R., 2001, "Modeling of the mechanical effects induced by the tungsten inert-gas welding of the IN718 superalloy," *Metallurgical and Materials Transactions A*, 32(7), pp. 1713-1725.
- [20] Liu, C., Wu, B., and Zhang, J., 2010, "Numerical Investigation of Residual Stress in Thick Titanium Alloy Plate Joined with Electron Beam Welding," *Metallurgical and Materials Transactions B*, 41(5), pp. 1129-1138.
- [21] Zäh, M. F., and Lutzmann, S., 2010, "Modelling and simulation of electron beam melting," *Production Engineering. Research and Development*, 4, pp. 15-23.
- [22] Roberts, I. A., Wang, C. J., Esterlein, R., Stanford, M., and Mynors, D. J., 2009, "A three-dimensional finite element analysis of the temperature field during laser melting of metal powders in additive layer manufacturing," *International Journal of Machine Tools and Manufacture*, 49(12-13), pp. 916-923.

- [23] Lin, T. H., Watson, J. S., and Fisher, P. W., 1985, "Thermal conductivity of iron-titanium powders," *Journal of Chemical & Engineering Data*, 30(4), pp. 369-372.
- [24] Sih, S. S., and Barlow, J. W., 2004, "The prediction of the emissivity and thermal conductivity of powder beds," *Particulate Science and Technology*, 22, pp. 291-304.
- [25] Kolossov, S., Boillat, E., Glardon, R., Fischer, P., and Locher, M., 2004, "3D FE simulation for temperature evolution in the selective laser sintering process," *International Journal of Machine Tools and Manufacture*, 44(2-3), pp. 117-123.
- [26] Patil, R. B., and Yadava, V., 2007, "Finite element analysis of temperature distribution in single metallic powder layer during metal laser sintering," *International Journal of Machine Tools and Manufacture*, 47(7-8), pp. 1069-1080.
- [27] Tolochko, N. K., Arshinov, M. K., Gusarov, A. V., Titov, V. I., Laoui, T., and Froyen, L., 2003, "Mechanisms of selective laser sintering and heat transfer in Ti powder," *Rapid Prototyping Journal*, 9, pp. 314-326.
- [28] Sun, S., Zheng, L., Liu, Y., Liu, J., and Zhang, H., 2015, "Selective laser melting of Al-Fe-V-Si heat-resistant aluminum alloy powder: modeling and experiments," *The International Journal of Advanced Manufacturing Technology*, pp. 1-11.
- [29] Arafin, M., Medraj, M., Turner, D., and Bocher, P., 2007, "Transient liquid phase bonding of Inconel 718 and Inconel 625 with BNi-2: Modeling and experimental investigations," *Materials Science and Engineering: A*, 447(1), pp. 125-133.
- [30] Kamnis, S., Gu, S., and Zeoli, N., 2008, "Mathematical modelling of Inconel 718 particles in HVOF thermal spraying," *Surface and Coatings Technology*, 202(12), pp. 2715-2724.
- [31] Wang, L., Felicelli, S., Gooroochurn, Y., Wang, P. T., and Horstemeyer, M. F., 2008, "Optimization of the LENS process for steady molten pool size," *Materials Science and Engineering A*, 474, pp. 148-156.
- [32] Lundbäck, A., Alberg, H., and Henrikson, P., "Simulation and validation of TIG welding and post weld heat treatment of an Inconel 718 plate," *Mathematical Modelling of Weld Phenomena 7*, pp. 683-696.
- [33] Hussein, A., Hao, L., Yan, C., and Everson, R., 2013, "Finite element simulation of the temperature and stress fields in single layers built without-support in selective laser melting," *Materials & Design*, 52, pp. 638-647.
- [34] Price, S., Cheng, B., Lydon, J., Cooper, K., and Chou, K., 2014, "On Process Temperature in Powder-Bed Electron Beam Additive Manufacturing: Process Parameter Effects," *Journal of Manufacturing Science and Engineering*, 136(6), pp. 061019-061019.
- [35] Cheng, B., Gong, X., Xiaoqing, W., and Chou, K., 2014, "Thermal Analysis, Microstructural Characterization And Nanoindentation For Electron Beam Additive Manufacturing," *ASME District F Early Career Technical Conference, Birmingham, AL, November 1-2, 2014*.
- [36] Cheng, B., and Chou, K., 2014, "Thermal Stresses Associated with Part Overhang Geometry in Electron Beam Additive Manufacturing: Process Parameter Effects," *25th Annual International Solid Freeform Fabrication Symposium - An Additive Manufacturing Conference, Austin, TX, USA, August 4-6, 2014*.
- [37] Cheng, B., and Chou, K., 2013, "Melt Pool Geometry Simulations for Powder-Based Electron Beam Additive Manufacturing," *24th Annual International Solid Freeform Fabrication Symposium - An Additive Manufacturing Conference, Austin, TX, USA, August 12-14, 2013*.